

Magnetism on ideal triangular lattices in NaBaYb(BO₃)₂Shu Guo,¹ A. Ghasemi,² C. L. Broholm,² and R. J. Cava^{1,*}¹Department of Chemistry, Princeton University, Princeton, New Jersey 08544, USA²Institute for Quantum Matter and Department of Physics and Astronomy, Johns Hopkins University, Baltimore, Maryland 21218, USA

(Received 6 June 2019; published 10 September 2019)

We report the anisotropic magnetic properties of single crystals of the triangular lattice magnet NaBaYb(BO₃)₂. In this material, a layered [Yb(BO₃)₂]_∞ framework is sandwiched by Na⁺ or Ba²⁺ layers in alternation. The space group is centrosymmetric, $R\bar{3}m$, with no detectable disorder and Yb³⁺-based easy axis Kramers doublets forming layered triangular lattice planes. A specific-heat anomaly indicates a second-order phase transition at $T = 0.41(2)$ K that is suppressed to less than 0.15 K in a 0.1-T magnetic field. With a change in entropy of only 0.6(2)% of $R \ln 2$ at this transition, NaBaYb(BO₃)₂, however, retains 94(1)% of $R \ln 2$ entropy to the lowest temperature accessed ($T = 0.15$ K). Strong frustration and the potential for quantum magnetism are implied.

DOI: 10.1103/PhysRevMaterials.3.094404

I. INTRODUCTION

Geometric magnetic frustration occurs when interactions between magnetic spins compete and cannot be simultaneously satisfied. It is commonly found in materials with triangle-based or tetrahedron-based magnetic units [1–5]. Depending on the arrangements of these simple units, various geometrically frustrated frameworks, such as two-dimensional (2D) triangular lattices [6–9], kagome lattices [10–12], three-dimensional (3D) pyrochlore lattices [13], and hyperkagome lattices [14,15], are found. Unconventional magnetic ground states have been found in geometrically frustrated magnets (GFM), such as spin ice and quantum spin liquid states [16–18]. In general, the quantum states are most likely to be found in low-spin GFMs.

Recently, 2D magnetic systems based on rare-earth ions have received a significant amount of attention. For the current context the ongoing debate about spin liquid vs spin-glass behavior in the Yb-based layered triangular lattice material YbMgGaO₄, is of interest. The debate arises at a fundamental level from the fact that in the crystal structure of YbMgGaO₄ Mg and Ga atoms are randomly mixed in the same Wyckoff position, in equal proportion, with the magnetic Yb's positionally displaced from their ideal sites, making the low-temperature spin state, the result of interactions on the order of several degrees Kelvin in energy, disrupted by random magnetic bond disturbances of the same magnitude [19–23].

Hence the discovery of a structurally perfect, low-spin triangular lattice magnet based on the rare-earth ion Yb is of interest for further experimental and theoretical research. Considering the strong spin-orbit coupling and highly anisotropic magnetic properties among rare-earth (R) based materials, we have studied R -based triangular lattice materials that carry $4f$ electrons, including KBaR(BO₃)₂ [24,25] and RbBaR(BO₃)₂ [26]. The former materials have a symmetric

rare-earth triangular lattice, but the K and Ba atoms, which are in sites near the magnetic R ions, are disordered in the crystal structure, as is found for YbMgGaO₄. For RbBaR(BO₃)₂, on the other hand, although the Rb and Ba are structurally ordered, the R atoms are located on a geometrically distorted triangular lattice, which can introduce anisotropy in the magnetic interactions, again a nonideal case. In contrast, here we report the magnetic properties of a structurally ideal Yb-based triangular lattice magnet, NaBaYb(BO₃)₂, where single-crystalline samples can be grown with no detectable structural distortion or disorder. We report the absence of a conventional magnetic phase transition to a temperature of 0.15 K.

II. EXPERIMENTAL

A. Crystal growth of NaBaYb(BO₃)₂

NaF, Yb₂O₃, Na₂CO₃, BaCO₃, and H₃BO₃ were used as received. All starting materials were analytical grade and from commercial sources. Single crystals were obtained by high-temperature flux growth through spontaneous crystallization. Mixtures of Na₂CO₃/BaCO₃/Yb₂O₃/H₃BO₃/NaF with molar ratios of 3:2:1:[7-9]:[1-3] were fully ground and placed in a 10-ml platinum crucible. The crucible was rapidly heated to 960 °C in an electric furnace and held for 2 days until the melts became transparent and homogeneous. The solution was cooled slowly at a rate of 1–3 °C/h during the process of crystal growth and after melt solidification (~800 °C) cooled to room temperature at a rate of 25 °C h⁻¹. Millimeter-level hexagonal plate crystals (Fig. 1) were obtained at the top of solidified flux, from which they were mechanically separated. The remnant flux was cleaned from the crystals by washing with distilled water and ethanol in succession.

B. Single-crystal and powder x-ray diffraction

The crystal structure of the title compound was determined by single-crystal x-ray diffraction (SXRD). The diffraction

*Corresponding author: rcava@princeton.edu

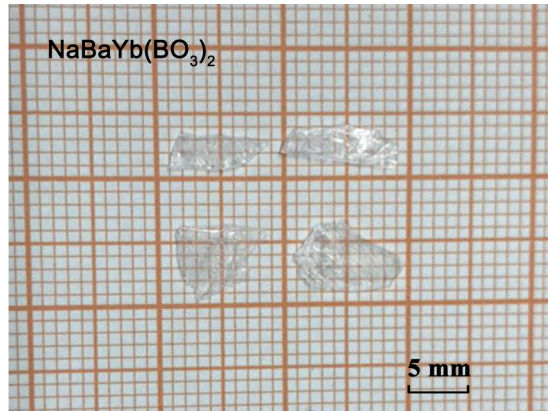


FIG. 1. NaBaYb(BO₃)₂ crystals grown by spontaneous nucleation.

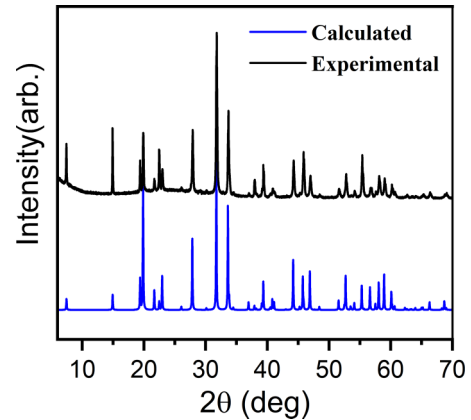


FIG. 2. Calculated and experimental PXRD patterns for crushed single crystals of NaBaYb(BO₃)₂.

data were collected at 299(1) K with a Kappa Apex2 CCD diffractometer (Bruker) using graphite-monochromated Mo-K α radiation ($\lambda = 0.71073 \text{ \AA}$). The raw data were corrected for background, polarization, and the Lorentz factor and multiscan absorption corrections were applied. Finally, the structure was analyzed by the intrinsic phasing method provided by the SHELXT structure solution program [27] and refined using the SHELXL least-squares refinement package with the OLEX2 program [28]. The ADDSYM algorithm in program PLATON was used to double check for possible higher symmetry [29], which was not found. For general analysis, crystals ground into a powder were characterized by powder x-ray diffraction (PXRD) on a Bruker D8 Advance Eco instrument in Bragg-Brentano geometry with Cu K α radiation ($\lambda = 1.5418 \text{ \AA}$) and a LynxEye-XE detector at room temperature in a range of $2\theta = 5\text{--}70^\circ$.

TABLE I. Crystal data and ambient temperature crystal structure refinements for NaBaYb(BO₃)₂.

Formula	NaBaYb(BO ₃) ₂
Formula mass (amu)	450.99
Crystal system	Trigonal
Space group	<i>R</i> -3 <i>m</i>
<i>a</i> (Å)	5.3295(3)
<i>c</i> (Å)	35.5840(17)
<i>V</i> (Å ³)	875.30(8)
<i>Z</i>	6
<i>T</i> (K)	299(1)
ρ (calcd)(g/cm ³)	5.133
λ (Å)	0.71073
<i>F</i> (000)	1170
θ (deg)	3.44–27.46
Crystal size (mm ³)	0.025 × 0.063 × 0.066
μ (mm ⁻¹)	22.672
<i>R</i> ₁ (obs)	0.0202
<i>R</i> ₁ (all Fo)	0.0205
<i>R</i> ₂ (all Fo)	0.0530
Residual electron density/(e Å ⁻³)	-2.485 to 1.347
Goodness of fit	1.163

C. Physical property measurements

Magnetization data were acquired using a Quantum Design physical property measurement Dynacool system (PPMS) equipped with a vibrating sample magnetometer option. Anisotropic magnetization data were obtained on single crystals. For the field-dependent magnetization at 1.8 K, when *H*||*c* and *H*⊥*c*, single crystals were mounted on a silica sample holder with GE varnish. Anisotropic temperature-dependent magnetization was measured between 1.8 and 300 K collected on visually oriented single-crystal samples in an applied field of *H* = 5000 Oe. Magnetic susceptibility χ was defined as *M*/*H*. The heat capacity was measured on a single crystal of NaBaYb(BO₃)₂ in the same PPMS instrument equipped with a ³He refrigerator in the temperature range 0.35–10 K. Lower-temperature specific-heat data were obtained down to *T* = 0.15 K using a dilution fridge insert in a PPMS.

III. RESULTS

A. Crystal growth and crystal structure

A 6 × 5 × 0.5–mm³ NaBaYb(BO₃)₂ crystal was successfully grown, as were smaller crystals in the same batch (Fig. 1). Observed and calculated PXRD patterns are shown in Fig. 2, confirming the single-phase nature of the samples

TABLE II. Wyckoff positions, coordinates, occupancies, and equivalent isotropic displacement parameters, respectively, for NaBaYb(BO₃)₂.

Atoms	Wyck site	<i>x/a</i>	<i>y/b</i>	<i>z/c</i>	S.O.F.	<i>U</i> _{eq}
Yb1	3 <i>b</i>	0	0	1/2	1	0.0069(2)
Yb2	3 <i>a</i>	0	0	0	1	0.0076(2)
Ba1	6 <i>c</i>	0	0	0.10220(2)	1	0.0101(2)
Na1	6 <i>c</i>	0	0	0.3822(3)	1	0.0336(16)
B1	6 <i>c</i>	0	0	0.2049(4)	1	0.013(3)
B2	6 <i>c</i>	0	0	0.2945(4)	1	0.011(3)
O1	18 <i>h</i>	0.4802(6)	0.5198(6)	0.37239(15)	1	0.0389(15)
O2	18 <i>h</i>	0.5185(5)	0.4815(5)	0.12789(14)	1	0.0165(10)

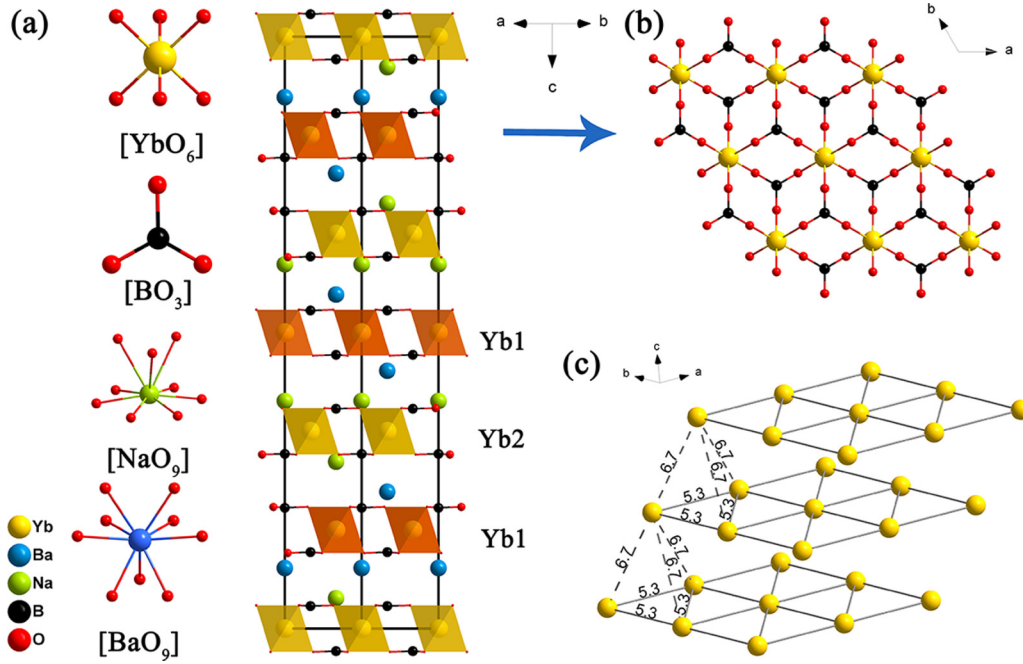


FIG. 3. (a) The crystal structure and building blocks of NaBaYb(BO₃)₂. (b) 2D structure formed by [YbO₆] and BO₃ groups, as viewed along the *c* axis. (c) The Yb-based triangular magnetic lattice, with the nearest-neighbor Yb³⁺ ions in the same plane (5.3 Å) and the neighboring plane (6.7 Å).

employed for the property measurements. NaBaYb(BO₃)₂ crystallizes in the centrosymmetric space group *R*-3*m* (no. 166). In the asymmetric unit of NaBaYb(BO₃)₂, there are two unique types of Yb atoms (Wyckoff sites 3*a* and 3*b*), with no variable structural parameters, i.e., the positions are fully fixed by the crystal symmetry to be in a perfect triangular lattice. The special positions of the Yb atoms create layers of ideal equilateral triangles. The two types of Yb atom layers have the same Yb-Yb in-plane and plane-to-plane separations. Also, there is one type of Na atom (Wyckoff site 6*c*), one type of Ba atom (Wyckoff site 6*c*), two types of B atoms (Wyckoff site 6*c*), and two types of O atoms (Wyckoff site 18*h*). The crystal structure is fully ordered, both positionally and chemically. The Yb³⁺ ions are in octahedral coordination with oxygen, with a regular [YbO₆] octahedral shape, and bond lengths $d_{\text{Yb1-O2}} = 2.197(5)$ Å and $d_{\text{Yb2-O1}} = 2.212(6)$ Å (i.e., to the number of significant digits relevant to the bonding 2.20 and 2.21 Å, respectively.) The [YbO₆] octahedra are connected through planar [BO₃] triangles in the *ab* plane, forming a layered [Yb(BO₃)₂]_∞ (i.e., 2D) framework [Fig. 3(b)]. One of the Yb layers has adjacent Na layers while the other has adjacent Ba layers. The Yb-based triangular lattices display ABCABC stacking (fcc-like) along the *c* axis of the

rhombohedral cell [Fig. 3(a)], with a Yb-Yb separation between layers of 6.7 Å, substantially larger than the in-plane Yb separation, 5.3 Å. The nine-coordinated Ba atoms and nine-coordinated Na atoms are situated in the space between adjacent Yb-based ideal triangular [Yb(BO₃)₂]_∞ planes. The crystallographic information, position, and selected bond lengths are summarized in Tables I–III.

B. Magnetic properties

The susceptibilities were fit to the Curie-Weiss law, $\chi - \chi_0 = C/(T - \Theta_{\text{CW}})$, where χ is the susceptibility, C is the Curie constant, Θ_{CW} is the Curie-Weiss temperature, and χ_0 is a temperature-independent contribution. The effective magnetic moments were then obtained using $\mu_{\text{eff}} = \sqrt{8C}$ (CGS units). Crystal-field effects influence the multiplet populations vs temperatures and thereby impact susceptibility measurements; therefore, the magnetic data were fit to the Curie-Weiss law at both low and high temperatures for comparison. The results for the high-temperature ($T = 150$ – 280 K) fits and low-temperature ($T = 1.8$ – 25 K) fits are listed in Table IV.

Direction-dependent magnetic susceptibility measurements were performed on a single crystal of NaBaYb(BO₃)₂. As shown in Fig. 4(a), the temperature-dependent susceptibility of NaBaYb(BO₃)₂ has uniaxial easy axis anisotropy $\chi_{(H\parallel c)} > \chi_{(H\perp c)}$. From the high-temperature fitting, the Curie-Weiss temperatures in different directions are $\Theta_{\text{CW}(H\perp c)} = -248.8$ K and $\Theta_{\text{CW}(H\parallel c)} = -30.7$ K, respectively. The negative Curie-Weiss temperatures in these fits are indicative of the crystal-field energy scale rather than intersite interactions. The effective magnetic moments of NaBaYb(BO₃)₂ for $H\parallel c$ and $H\perp c$ are $6.22 \mu_B/\text{Yb}$ and $3.80 \mu_B/\text{Yb}$, respectively. The large difference of effective magnetic moment

TABLE III. Selected bond lengths (Å) for NaBaYb(BO₃)₂.

Bond	Length	Bond	Length
(B1-O2) × 3	1.368(5)	(Ba1-O1) × 3	2.831(6)
(B2-O1) × 3	1.356(6)	(Ba1-O2) × 6	2.822(1)
(Yb1-O2) × 6	2.197(5)	(Na1-O1) × 6	2.694(1)
(Yb2-O1) × 6	2.212(6)	(Na1-O2) × 3	3.211(10)

TABLE IV. Effective moments (μ_{eff}) and Weiss temperatures (Θ_{CW}) for an NaBaYb(BO₃)₂ single crystal determined by fitting of the Curie-Weiss law to the magnetic susceptibility data in an applied field of 5 kOe. $\mu_{\text{FI}} = g_J \sqrt{J(J+1)}$ is the free ion magnetic moment where $J = \frac{7}{2}$ and $g_J = \frac{8}{7}$.

Direction	High- T fit	μ_{eff} (μ_B)	Θ_{CW} (K)	Low- T fit	μ_{eff} (μ_B)	Θ_{CW} (K)	M_{FI} (μ_B)
$H \perp c$	100–280 K	6.22	−248.80		1.78	−0.03	4.53
$H \parallel c$		3.80	−30.69	1.8–25 K	2.94	−0.15	
Ave		4.64	−113.45		2.23	−0.069	

between these two orientations is attributed to the structural anisotropy via crystal-field effects. In the low-temperature range fits, very small negative Curie-Weiss temperatures were observed for both field parallel to c and field perpendicular to c [$\Theta_{\text{CW}}(H \perp c) = -0.03$ K and $\Theta_{\text{CW}}(H \parallel c) = -0.15$ K].

Considering the trigonal crystal system, the weighted average magnetic susceptibility $\chi_{\text{ave}} = (2\chi_{(H \perp c)} + \chi_{(H \parallel c)})/3$. A linear Curie-Weiss fit was also applied to the weighted average data in both temperature ranges. At high temperature, the inverse susceptibility data give $\Theta_{\text{CW}} = -113.5$ K and $\mu_{\text{eff}} = 4.64 \mu_B/\text{Yb}$. The effective magnetic moment matches well with the expected value for free Yb³⁺ (4.53 μ_B). In contrast, in the low-temperature range (1.8–25 K), the Curie-Weiss fit yielded the $\Theta_{\text{CW}} = -0.07$ K and $\mu_{\text{eff}} = 2.23 \mu_B/\text{Yb}$. The effective magnetic moment (2.23 μ_B/Yb) is smaller than the value for free Yb³⁺ (4.53 μ_B) as a result of crystal-field effects. The field-dependent magnetization at 1.8 K shows a nonlinear response and saturates below 90 000 Oe to about 1.09 and 1.71 μ_B/Yb for $H \perp c$ and $H \parallel c$, respectively [Fig. 4(b)]. The implication is that additional steps in the magnetization will occur at higher applied fields. As shown in Fig. 5, the field-cooled (FC) and zero-field-cooled (ZFC) susceptibilities were measured on a powder sample at applied field of 100 Oe. The magnetic susceptibilities for both FC and ZFC increase down to 1.7 K without bifurcation, which indicates the absence of a spin-glass transition down to that temperature.

C. Specific heat

Specific-heat measurements were performed on a 1.2-mg single crystal. The nonmagnetic compound NaBaLu(BO₃)₂ was grown and its specific heat measured and used to isolate the magnetic contribution to the specific heat of

NaBaYb(BO₃)₂. At zero field, the magnetic specific heat C_m of NaBaYb(BO₃)₂ increases gradually upon cooling without a large anomaly characteristic of a conventional magnetic phase transition [Fig. 6(a)]. We shall later discuss a weak anomaly at $T = 0.41(2)$ K. When we apply fields of 0.1 and 0.5 T, however, a large upturn is induced at low temperatures. A broad peak is observed when the applied field exceeds 1 T. The broad peak moves to higher temperature with increasing field. The inset to Fig. 6(b) shows the change in entropy inferred from the data. At high fields the full value of $\Delta S_m = R \ln 2$ is obtained while at zero field the spin system retains 94(1)% of the $R \ln 2$ magnetic entropy down to $T = 0.15$ K.

Figure 6(b) shows a scaling plot of C_m vs $T/\mu H$. Here $\mu_{\text{sat},c} = 1.71 \mu_B/\text{Yb}$ is the saturation magnetization for $H \parallel c$. The scaling collapse for $H > 0.5$ T shows that the effect of intersite interactions is less than an energy of $\mu_{\text{sat},c} \times 0.5$ T = 0.57 K, which is consistent with $\Theta_{\text{CW}}(H \parallel c) = -0.15$ K inferred from the low- T susceptibility data. The solid line was calculated for a Kramers doublet. The excellent agreement with the data is evidence for a monodisperse ensemble Kramers doublets with saturation magnetization μ . Kramers doublets are characterized by the following dimensionless ratio: $R \equiv (\frac{\mu_{\text{eff}}}{\mu_{\text{sat}}})^2 = 3$. For comparison this squared moment ratio, inferred from our susceptibility and saturation magnetization measurements, is $R_{\parallel c} = 2.96$ and $R_{\perp c} = 2.67$ for $H \parallel c$ and $H \perp c$, respectively. The deviations below 3 are within the systematic uncertainty associated with sample alignment in the different measurements and at the different fields. Specifically, torque and sample misalignment tend to overestimate the hard axis saturation magnetization and thus suppress $R_{\perp c}$ below 3.

Figure 6(c) shows the low-temperature dilution fridge data in greater detail. An anomaly at $T_c = 0.41(2)$ K is clearly

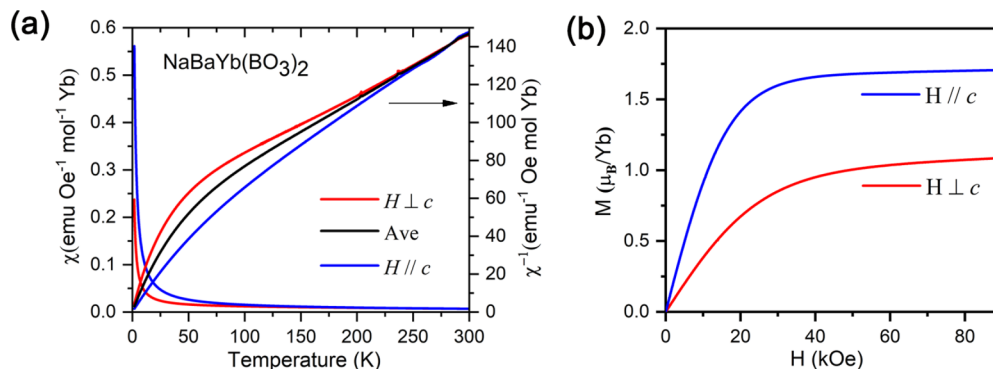


FIG. 4. Magnetic characterization of single-crystal NaBaYb(BO₃)₂. (a) Anisotropic and polycrystalline averaged inverse magnetic susceptibility and (b) 1.8-K field-dependent magnetization measurements on a single crystal parallel and perpendicular to the c axis.

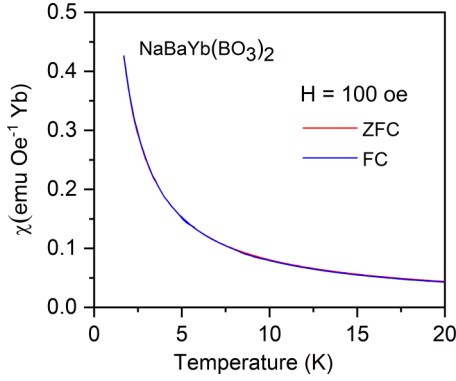


FIG. 5. FC and ZFC magnetic susceptibility in an applied field of 100 Oe for $\text{NaBaYb}(\text{BO}_3)_2$.

visible both in adiabatic heat pulse and long pulse measurements. Their consistency rules out a first-order phase transition in the $T > 0.15$ -K temperature range accessed. The total change in entropy through this apparent second-order phase transition is only $\Delta S = 0.006(2)R \ln 2$, leaving much entropy for a lower-temperature phase transition, a crossover to a nondegenerate state, or a nonergodic manifold.

IV. DISCUSSION

We first discuss the nature of the spin degrees of freedom. The scaling collapse of the high-field specific-heat data indicates that Yb^{3+} forms low-energy Kramers doublets as anticipated given the $\bar{3}m$ point-group symmetry. In combination, the high-field magnetization and the low-field susceptibility measurements constrain the ratio between the Kramers doublet moment of the two Yb sites. Denote $\mu_{\text{sat},2} = f\mu_{\text{sat},1}$. For any field direction and each site $i = 1, 2$ we have $\mu_i = \mu_{\text{sat},i} \tanh \beta \mu_{\text{sat},i} B$, which implies $\chi_i = \frac{\mu_{\text{sat},i}^2}{k_B T} \equiv \frac{\mu_{\text{eff},i}^2}{3k_B T}$ and $R_i = \left(\frac{\mu_{\text{eff},i}}{\mu_{\text{sat},i}}\right)^2 = 3$. For the sample average we have $\mu_{\text{sat}} = \frac{1}{2}\mu_{\text{sat},1}(1+f)$ while $\mu_{\text{eff}}^2 = \frac{1}{2}\mu_{\text{eff},1}^2(1+f^2)$ because $\chi = \frac{1}{2}(\chi_1 + \chi_2)$. Thus $R = \left(\frac{\mu_{\text{eff}}}{\mu_{\text{sat}}}\right)^2 = 6 \frac{1+f^2}{(1+f)^2}$ so that $3 \leq R \leq 6$, the limits realized for $f = 1$ and $0, \infty$ respectively. Considering systematic errors, our data place an upper limit of $R < 3.05$ on the two crystallographic directions from which we obtain $0.77 < f < 1.3$. Thus, the saturation moments of the two Yb sites cannot differ significantly ($< 25\%$) from each other either for $H \parallel c$ or for $H \perp c$. Given the measured easy axis anisotropy this implies that both Yb^{3+} sites must be easy axis pseudo-spin-1/2 degrees of freedom. A full determination of the ground-state spin-orbital wave function of Yb^{3+} will require measurements of the crystal-field level scheme, for example, through inelastic neutron scattering.

Next, we discuss the nature and strength of intersite interactions. Considering first the dipole-dipole interaction, the relevant nearest-neighbor bond energy scale is $D = \frac{\mu_0 \mu_{\text{sat},c}^2}{4\pi a^3} = 12$ mK. For comparison the bond energy scale inferred from the low- T Curie-Weiss fit along the c axis is $\tilde{J} = \frac{\Theta_{\text{CW},c}}{z} \left(\frac{g_J \mu_B}{\mu_{\text{sat},c}}\right)^2 = 11$ mK. Here we have used the Landé factor $g_J = \frac{8}{7}$ and the coordination number $z = 6$. Note that all spin-spin interactions contribute to Θ_{CW} and can cancel so

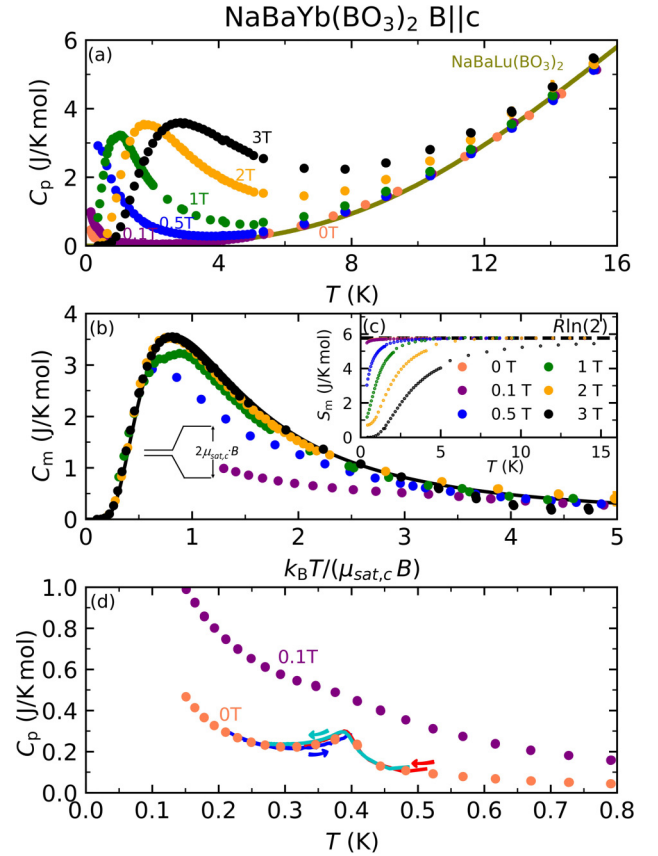


FIG. 6. (a) Heat capacity C_p as a function of temperature for an $\text{NaBaYb}(\text{BO}_3)_2$ single crystal measured under several applied magnetic fields. Data for the nonmagnetic analog $\text{NaBaLu}(\text{BO}_3)_2$, employed for subtraction of the phonon contribution, are also shown (b), with C_m/T as a function of temperature at several magnetic fields scaled vs $k_B T / (\mu_{\text{sat},c} B)$ where k_B is the Boltzmann constant, B is the applied magnetic field along the c axis, and $\mu_{\text{sat},c} = 1.71 \mu_B/\text{Yb}$ is the corresponding saturation moment. (c) Change in entropy vs temperature shifted to accommodate the full $R \ln 2$ spin entropy in the high- T limit for consistency with the ground-state Kramers degeneracy. (d) The very-low-temperature heat capacity measured in zero field and a field of 0.1 T. A small anomaly at 0.41(2) K indicates a second-order phase with $\Delta S = 0.006(2)R \ln 2$. Points were obtained with the heat pulse method, while continuous lines were obtained with the long pulse method upon heating and cooling as indicated by the arrows.

that naïve interpretation of Θ_{CW} can underestimate exchange interactions. Nonetheless the similarity of these energy scales suggests dipole interactions are significant in the magnetism of $\text{NaBaYb}(\text{BO}_3)_2$. Even in NaYbO_2 , where just one O is in the superexchange path and thus favoring exchange, one finds $D \sim \tilde{J}$ [30]. Since the spacing between Yb in adjacent layers (6.7 Å) exceeds the in-plane spacing (5.3 Å) the nearest-neighbor interlayer dipole interactions (which link the triangular lattices as in a 3D fcc lattice) are a factor $\left(\frac{6.7}{5.3}\right)^3 = 2.0$ weaker than the corresponding intralayer interaction.

V. CONCLUSIONS

In summary, single crystals of the structurally perfect Yb-based triangular lattice magnet $\text{NaBaYb}(\text{BO}_3)_2$ have

been grown by the spontaneous nucleation method. According to the SXRD refinement, the crystal structure of $\text{NaBaYb}(\text{BO}_3)_2$ is fully crystallographically ordered, forming a 2D $[\text{Yb}(\text{BO}_3)_2]_\infty$ triangular framework with no structural disorder. The magnetism arises from pseudo-spin-1/2 quantum degrees of freedom with $\sim 60\%$ enhanced c axis moment in both of two distinct triangular lattices. A small anomaly in the specific heat at $T = 0.41(2)$ K signals a second-order phase transition that is associated with a change in entropy of just $\Delta S = 0.006(2)R \ln 2$. The preponderance of the magnetic entropy is, however, unaccounted for at zero field down to the

lowest temperature of the present experiment ($T = 0.15$ K), leaving open the possibility of exotic magnetism arising from easy axis quantum spins with frustrated long-range, possibly dipolar, interactions on the triangular lattice [31].

ACKNOWLEDGMENT

This work was supported as part of the Institute for Quantum Matter, an Energy Frontier Research Center funded by the U.S. Department of Energy, Office of Science, Basic Energy Sciences under Award No. DE-SC0019331.

-
- [1] C. Lacroix, P. Mendels, and F. Mila, *Introduction to Frustrated Magnetism* (Springer-Verlag, Berlin, 2011).
- [2] H. Takagi and S. Niitaka, *Highly Frustrated Magnetism in Spinels* (Springer-Verlag, Berlin, 2011).
- [3] D. W. Bruce, D. O'Hare, and R. I. Walton, *Geometrically Frustrated Magnetic Materials* (Wiley, New York, 2010), Chap. 2.
- [4] R. Becker, M. Johnsson, R. K. Kremer, H.-H. Klauss, and P. Lemmens, *J. Am. Chem. Soc.* **128**, 15469 (2006).
- [5] X.-Y. Wang and S. C. Sevov, *Chem. Mater.* **19**, 3763 (2007).
- [6] D. Weber, L. M. Schoop, D. Wurmbrand, J. Nuss, E. M. Seibel, F. F. Tafti, H. Ji, R. J. Cava, R. E. Dinnebier, and B. V. Lotsch, *Chem. Mater.* **29**, 8338 (2017).
- [7] Y. Shimizu, K. Miyagawa, K. Kanoda, M. Maesato, and G. Saito, *Phys. Rev. Lett.* **91**, 107001 (2003).
- [8] M.-H. Whangbo, D. Dai, K.-S. Lee, and R. K. Kremer, *Chem. Mater.* **18**, 1268 (2006).
- [9] M. Xia, K. Zhai, J. Lu, Y. Sun, and R. K. Li, *Inorg. Chem.* **56**, 8100 (2017).
- [10] Y. Tang, C. Peng, W. Guo, J.-f. Wang, G. Su, and Z. He, *J. Am. Chem. Soc.* **139**, 14057 (2017).
- [11] L. Santos, M. A. Baranov, J. I. Cirac, H.-U. Everts, H. Fehrmann, and M. Lewenstein, *Phys. Rev. Lett.* **93**, 030601 (2004).
- [12] M. P. Shores, E. A. Nytko, B. M. Bartlett, and D. G. Nocera, *J. Am. Chem. Soc.* **127**, 13462 (2005).
- [13] S. T. Bramwell and M. J. Gingras, *Science* **294**, 1495 (2001).
- [14] G. Chen and L. Balents, *Phys. Rev. B* **78**, 094403 (2008).
- [15] T. Takayama, A. Yaresko, A. Matsumoto, J. Nuss, K. Ishii, M. Yoshida, J. Mizuki, and H. Takagi, *Sci. Rep.* **4**, 6818 (2014).
- [16] M. J. Harris, S. T. Bramwell, D. F. McMorrow, T. Zeiske, and K. W. Godfrey, *Phys. Rev. Lett.* **79**, 2554 (1997).
- [17] T. Fennell, P. Deen, A. Wildes, K. Schmalzl, D. Prabhakaran, A. Boothroyd, R. Aldus, D. McMorrow, and S. Bramwell, *Science* **326**, 415 (2009).
- [18] G. Ehlers, A. Cornelius, T. Fennell, M. Koza, S. Bramwell, and J. Gardner, *J. Phys. Condens. Matter* **16**, S635 (2004).
- [19] Y. Li, G. Chen, W. Tong, L. Pi, J. Liu, Z. Yang, X. Wang, and Q. Zhang, *Phys. Rev. Lett.* **115**, 167203 (2015).
- [20] J. A. Paddison, M. Daum, Z. Dun, G. Ehlers, Y. Liu, M. B. Stone, H. Zhou, and M. Mourigal, *Nat. Phys.* **13**, 117 (2017).
- [21] Y. Xu, J. Zhang, Y. S. Li, Y. J. Yu, X. C. Hong, Q. M. Zhang, and S. Y. Li, *Phys. Rev. Lett.* **117**, 267202 (2016).
- [22] Z. Zhu, P. A. Maksimov, S. R. White, and A. L. Chernyshev, *Phys. Rev. Lett.* **119**, 157201 (2017).
- [23] Y. Li, D. Adroja, R. I. Bewley, D. Voneshen, A. A. Tsirlin, P. Gegenwart, and Q. Zhang, *Phys. Rev. Lett.* **118**, 107202 (2017).
- [24] S. Guo, T. Kong, F. A. Cevallos, K. Stolze, and R. J. Cava, *J. Magn. Magn. Mater.* **472**, 104 (2019).
- [25] M. B. Sanders, F. A. Cevallos, and R. J. Cava, *Mater. Res. Express* **4**, 036102 (2017).
- [26] R. J. Cava and S. Guo, *Bull. Am. Phys. Soc.* **64**, G70.00164 (2019).
- [27] G. M. Sheldrick, *Acta Crystallogr. Sect. C* **71**, 3 (2015).
- [28] O. V. Dolomanov, L. J. Bourhis, R. J. Gildea, J. A. Howard, and H. Puschmann, *J. Appl. Crystallogr.* **42**, 339 (2009).
- [29] A. L. J. Spek, *J. Appl. Crystallogr.* **36**, 7 (2003).
- [30] L. Ding, P. Manuel, S. Bachus, F. Grubler, P. Gegenwart, J. Singleton, R. D. Johnson, H. C. Walker, D. T. Adroja, A. D. Hillier, and A. A. Tsirlin, [arXiv:1901.07810](https://arxiv.org/abs/1901.07810).
- [31] A. Keleş and E. Zhao, *Phys. Rev. Lett.* **120**, 187202 (2018).